

Article

Bacterial Detection and Differentiation of *Staphylococcus aureus* and *Escherichia coli* Utilizing Long-Period Fiber Gratings Functionalized with Nanoporous Coated Structures

Shuyue He ¹, Jue Wang ², Fan Yang ¹ , Tzu-Lan Chang ², Ziyu Tang ¹, Kai Liu ^{1,3}, Shuli Liu ^{4,5}, Fei Tian ¹, Jun-Feng Liang ², Henry Du ^{1,*} and Yi Liu ^{5,6,*}

¹ Department of Chemical Engineering and Materials Science, Stevens Institute of Technology, Hoboken, NJ 07030, USA

² Department of Chemistry and Chemical Biology, Stevens Institute of Technology, Hoboken, NJ 07030, USA

³ Department of Materials Research, Zhuzhou Cemented Carbide Cutting Tools Co., Ltd., Diamond Industrial Park, No. 28 South Huanghe Road, Tianyuan District, Zhuzhou 412007, China

⁴ National Innovation Center for Advanced Rail Transit Equipment, Zhuzhou 412001, China

⁵ Hunan Engineering Technology Research Center of Intelligent Sensing and Maintenance for Railway Transportation Equipment, Zhuzhou 412001, China

⁶ School of Mechanical Engineering and Mechanics, Xiangtan University, Xiangtan 411105, China

* Correspondence: hdu@stevens.edu (H.D.); liuyi@xtu.edu.cn (Y.L.)

Abstract: A biosensor utilizing long-period fiber gratings (LPFG) functionalized with nanoporous coated structures was developed for the rapid detection of *Staphylococcus aureus* (*S. aureus*) bacteria. The nanoporous structure coatings on the LPFG surface facilitated specific adhesion and interaction with *S. aureus*, resulting in an instantaneous shift in the resonance wavelength (RW) in the transmission spectrum of the LPFG. The LPFG with nanoporous polyelectrolyte coatings exhibited an approximately seven-fold RW shift compared to the bare LPFG under the optimal experiment conditions. By tracking the RW shifts, we were able to monitor the real-time *S. aureus* adhesion to study the interaction process in detail. The bacterial differentiation and *S. aureus* specificity of the method was confirmed through a series of studies using *Escherichia coli* (*E. coli*). This nanoporous structure-enabled LPFG-based biosensor scheme holds significant promise for rapid, reliable, and low-cost detection of *S. aureus* for biomedical applications.

Keywords: long-period fiber gratings; biosensor; nanoporous structure; *Staphylococcus aureus*; *Escherichia coli*



Citation: He, S.; Wang, J.; Yang, F.; Chang, T.-L.; Tang, Z.; Liu, K.; Liu, S.; Tian, F.; Liang, J.-F.; Du, H.; et al. Bacterial Detection and Differentiation of *Staphylococcus aureus* and *Escherichia coli* Utilizing Long-Period Fiber Gratings Functionalized with Nanoporous Coated Structures. *Coatings* **2023**, *13*, 778. <https://doi.org/10.3390/coatings13040778>

Academic Editor: Aldona Balčiūnaitė

Received: 2 March 2023

Revised: 5 April 2023

Accepted: 12 April 2023

Published: 17 April 2023



Copyright: © 2023 by the authors. Licensee MDPI, Basel, Switzerland. This article is an open access article distributed under the terms and conditions of the Creative Commons Attribution (CC BY) license (<https://creativecommons.org/licenses/by/4.0/>).

1. Introduction

Microorganisms are everywhere. Even though most bacteria are harmless, a few of them can cause serious illness and even death. Countless people are hospitalized each year as a result of bacteria-related infections [1–4]. In hospital settings, *Staphylococcus aureus* (*S. aureus*) is the primary sources of nosocomial infections [5]. Traditional, culture-based tests are time-consuming and can work poorly with slow-growing or viable but non-culturable organisms. They do not provide real-time results or timely information that is needed in applications such as industrial manufacturing. Rapid detection and differentiation of bacteria is crucial to identify and distinguish pathological differences, especially at the early stage of diagnosis [6], and to efficiently reduce their impact on human and animal health [7].

There are a variety of methods for bacteria detection based on bio-recognition strategies [8] such as nucleic acids (DNA/RNA) [9,10], bacteriophages [3,11] and antibodies [12,13]. Although nucleic acids and bacteriophages offer high specificity [8], these techniques are not only laborious and time-consuming, but also require highly trained personnel and dedicated facilities [14]. Even though antibody-based recognition methods are

sensitive [10], they are costly and may result in false positives due to cross-binding to other bacteria [11]. The fluorescent label method involves labeling with specific dyes, making the procedure complex and time-consuming [15]. Label-free biosensors are of significant appeal for rapid, reliable and in situ measurements [16]. Surface plasmon resonance (SPR)-based sensing is one of the most widely investigated label-free detection methods [17–26], but the sensor area and mass transport of this method are limited [27]. Recently, LPFG-based label-free biosensors have also been studied for bio-analyte detections [8,28]. As a low cost, simple detection technique, it offers the opportunity for rapid and reliable detections, even in harsh environments [29]. In the past few decades, numerous studies have focused on the development of biofunctional layer-by-layer (LbL) polyelectrolyte films [30–32]. The freedom in designing LbL films with multifunctionality shows particular potential in biomedical developments ranging from design of medical devices and drugs [33] to the study of bacterial behaviors [31]. The LbL multilayer coatings with three-dimensional structures can incorporate probes and molecular recognition elements to generate an amplified response and improve the sensitivity and selectivity of detection, opening up new opportunities for biosensors [34,35]. LPFG-based biosensors offer the capability to not only quantitatively measure changes in refractive index (RI) of the analyte under investigation, but also enable real-time analysis of dynamic interactions [36].

In this study, a cutting-edge optofluidic biosensor utilizing LPFG was developed for the swift detection of low-concentration *S. aureus* bacteria. First, functional polyelectrolyte coatings were deposited on the surface of LPFG via LbL assembly. Nano-structured pores were then introduced in these coatings through post-assembly treatment to facilitate *S. aureus* adhesion and hence its ready detection. We found that the LPFG with functional coatings containing nanopores exhibited around a seven-fold increase in RW shift as compared to the bare LPFG upon exposure to *S. aureus* for only 60 min. No apparent resonance wavelength (RW) shift change was observed when the same nanoporous coated LPFG was exposed to *E. coli*. The different adhesion behavior of bacteria on the porous structures coated for specific bacteria allows us to selectively detect and differentiate bacteria using nanoporous coated LPFG.

2. Results and Discussion

2.1. Characterization of Nanoporous [PAH/PAA]₁₀-PAH Coatings

The LbL films were assembled from poly(allylamine hydrochloride) (PAH) and poly(acrylic acid) (PAA). We prepared 10 bilayers of [PAH/PAA] and applied another PAH layer as the top layer of [PAH/PAA]₁₀ coating. The nanoporous structure was introduced to the coatings of [PAH/PAA]₁₀-PAH via acid corrosion. This process of transformation is substantial and irreversible, and results in the modification of the topography of PAH/PAA coatings to generate nanoporous structures [37]. The mechanism for this process involves a reduction in the ionic cross-link in the films followed by spinodal decomposition to generate thin films with a nanoporous morphology [37,38].

As shown in Figure 1, the COO[−] groups of PAA readily bind to the NH₃⁺ groups of PAH, forming −NHCO[−] ionic intermolecular cross-links (step 1). In the low-pH environment, the hydrogen cations protonate some of the COO[−] groups, leading to breakage of interchain ion pairs of LbL (step 2) and thus increased mobility of polymer chains (step 3). It allows more energetically favorable reorganizations of the chains on the surface. This reorganization results in an insoluble swelling polyelectrolyte complex (step 4), which is followed by phase separation in the neutral solution via a spinodal decomposition process [29,37], thus forming nanopores (step 5).

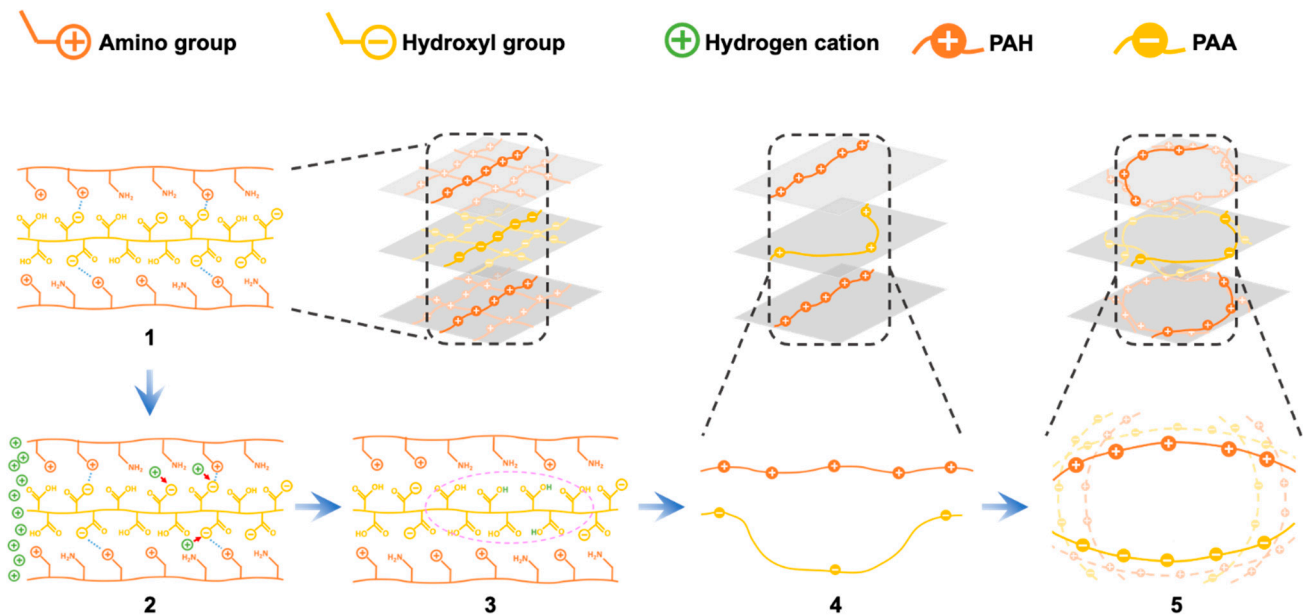


Figure 1. The mechanism of pH-induced nanoporous structure in the coating of [PAH/PAA]₁₀-PAH. Step 1 is the side view of the [PAH/PAA]₁₀-PAH coatings; in the dashed frame shown on the right is the pseudo-3D view. Step 2 and step 3 are side views showing the breakage of the interchain ionic bonds between amino groups and carboxylate groups due to protonation in acidic solution. Step 4 is the top view showing the formation of a swelling complex after ionic bonds break in acidic solution; the pseudo-3D view is shown in the dashed frame above. Step 5 is the top view showing the spinodal decomposition and nanopores formation in the neutral buffer solution; the pseudo-3D view is shown in the dash frame above.

Figure 2a depicts the SEM image of the nanoporous coating. Figure 2b shows the size distribution of the nanopores, with the majority falling into the size range from 200 to 400 nm. The average diameter of these nanopores is measured to be 300 ± 86.39 nm, which is slightly smaller than the physical dimensions of *S. aureus* and *E. coli*. The nanopores were investigated for their potential to provide protection to microorganisms against chemical exposure and hydrodynamic shear forces, [39,40], and thus provide bacterial retention on the surface of the designed functional polyelectrolyte coatings.

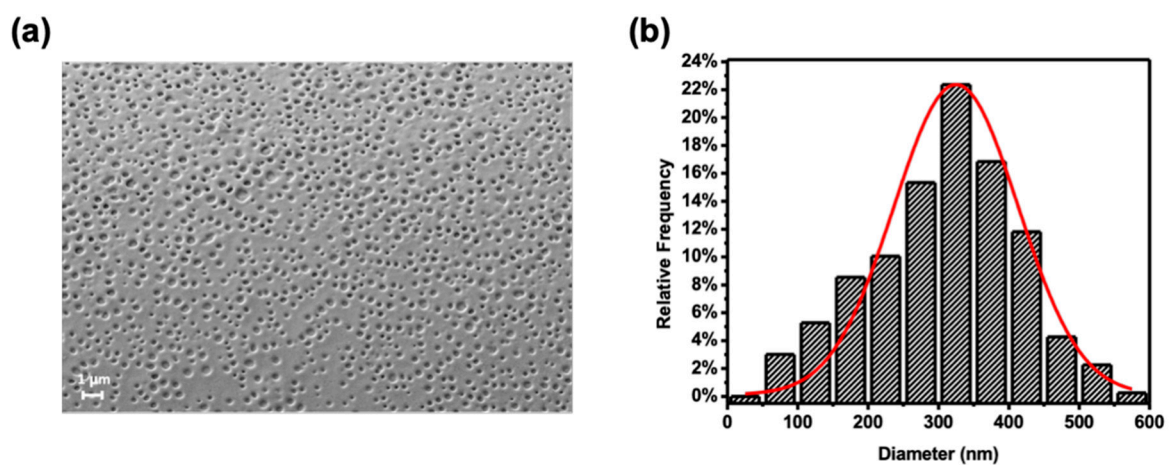


Figure 2. (a) The SEM image displays the pH-induced nanoporous structure of the coatings on the LPFG. (b) A statistical histogram illustrates the diameter distribution of the nanopores on the nanoporous coating.

2.2. Rapid Detection of Bacteria Using LPFGs with Functional Coatings

Prior to bacterial detection measurements, the RWs of the LPFGs with [PAH/PAA]₁₀-PAH and nanoporous functional coatings were measured at a flow rate of 30 $\mu\text{L}/\text{min}$ in PBS buffer solution (37 $^{\circ}\text{C}$) for 260 min. This assessment was made to determine the stability of the coatings in a microfluidic environment. The RWs of the LPFGs coated with [PAH/PAA]₁₀-PAH and nanoporous coatings exhibited consistent stability throughout the measurement period, with a maximum fluctuation of 0.05 nm, which is comparable to the resolution of the optical spectrum analyzer (OSA) at 0.05 nm. The stability of the coating of [PAH/PAA]₁₀-PAH and the nanoporous coatings can be ascribed to the chemical cross-linking mechanism achieved through a heat-induced amidation reaction, wherein the coatings were subjected to a temperature of 200 $^{\circ}\text{C}$ to facilitate the formation of amide cross-links ($-\text{NHCO}-$) between NH_3^+ groups of PAH and COO^- groups of PAA [15].

During the bacterial detection measurement, a syringe pump was utilized to continuously inject a fresh bacterial solution into the LOFOP. Assuming that the coverage density of the bacteria on the LPFG remains constant, the RI of the surrounding coating on the LPFG is not expected to undergo any changes [41]. When the coverage density of the bacteria changes, the surrounding RI of LPFG changes accordingly, leading to an RW shift in the transmission spectrum of the LPFG. The capacity to accurately track the RW shift, and thereby determine the coverage density of bacteria, enables us to investigate the dynamics of bacterial adhesion on functional coatings applied to the LPFG in situ.

For rapid bacterial detection, RW shifts of the coated LPFGs were captured at 10 min intervals over a period of 60 min. This was accomplished by exposing the LPFGs to bacterial solutions with a concentration of 10^4 CFU/mL in PBS, while maintaining a flow rate of 30 $\mu\text{L}/\text{min}$ and a temperature of 37 $^{\circ}\text{C}$. The reason we used 10^4 CFU/mL bacterial concentration is because it represents an infection of the urinary tract, and thus simplifies the experimental process [42]. Bacterial monitoring of LPFGs with various substrates was carried out three times for each substrate. Figure 3a shows the RW shifts of the bare LPFGs, [PAH/PAA]₁₀-PAH-coated LPFGs and nanoporous [PAH/PAA]₁₀-PAH-coated LPFGs for monitoring *S. aureus* (a spherical Gram positive (G+) microbe). As shown in Figure 3a, the fitted slopes of RW shifts for the bare LPFGs, the coatings and the nanoporous coatings were 0.45, 4.09 and 7.96 pm/min, respectively. The RW shift of the bare LPFGs was close to zero, due to the limited adhesion of bacteria on the bare LPFGs surface. As the bacteria were retained on the surface of the polyelectrolyte coatings, the effective external RI was changed and thus a corresponding red shift occurred in the RW of the LPFGs. Figure 3b–d are the overall SEM images of *S. aureus* on bare LPFGs, [PAH/PAA]₁₀-PAH-coated and nanoporous [PAH/PAA]₁₀-PAH-coated LPFGs at 60 min, respectively. The densities of bacteria attached to different platforms are shown in Figure S2. Figure 3b shows that there were few bacteria attached to the bare LPFGs after 60 min, which is consistent with its limited RW shift as shown in Figure 3a (blue square). For the *S. aureus* monitoring using coated LPFGs, as shown in Figure 3a (red circle), there was a striking 10-fold increase in the slope of the RW shift compared to that of the bare LPFGs. The SEM image (Figure 3c) clearly shows that there is an increase in the density of *S. aureus* on the coated LPFGs. The increased surface wettability of [PAH/PAA]₁₀-PAH-coated LPFGs [43] and the improved hydrophilicity [44] of the PAH-terminated substrate with amino groups may favor the adhesion of *S. aureus*, leading to an increased density of *S. aureus* and thus the enhanced sensitivity in terms of RW shifts. It was observed that the *S. aureus* were aggregated and attached to the coating surface as bacterial clusters. The clusters were due to microbial self-binding termed “autoaggregation”, a widespread phenomenon mediated by the surface proteins of bacteria [45]. The RW shift of nanoporous coated LPFGs shows the highest fitted slope when monitoring *S. aureus* (Figure 3a, orange triangle), with a 20-fold increase compared to that of the bare LPFGs. The transmission spectra of nanoporous coatings for *S. aureus* detection for the first 60 min are shown in Figure S3a. The SEM image of *S. aureus* attached to the nanoporous coatings (Figure 3d) clearly displays that the density of *S. aureus* on the nanoporous coating was higher than that on bare LPFGs (Figure 3b)

and the coated LPFGs (Figure 3c). The nanoporous structure of the coatings results in an enlarged surface area, which subsequently diminishes the shear stress encountered by the adhered bacteria in fluidic conditions [46,47], facilitating the adhesion of *S. aureus* and thus enhancing the RW shifts. As previously mentioned, the presence of the nanoporous structure in the coatings has been reported to offer protection to bacteria against chemical exposure and hydrodynamic shear forces within a fluidic system. This protective effect further facilitates bacterial adhesion onto the nanoporous coatings, ultimately enhancing the sensitivity of LPFGs for bacterial detection.

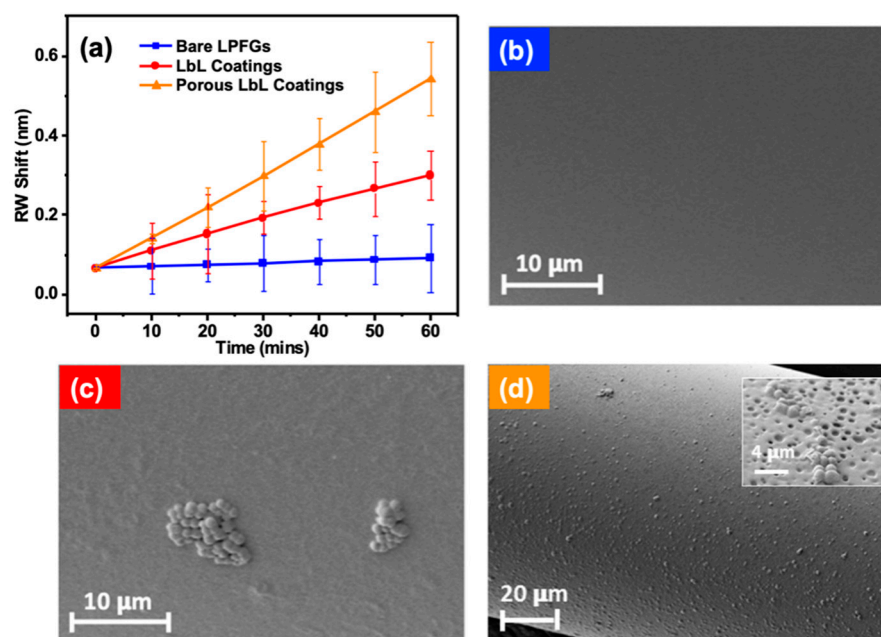


Figure 3. (a) The time-resolved RW shifts of the bare LPFGs, the $[\text{PAH}/\text{PAA}]_{10}$ -PAH-coated LPFGs and the nanoporous coated LPFGs for *S. aureus* detections at a flow rate of $30 \mu\text{L}/\text{min}$ and temperature of 37°C for 60 min. Each experiment was repeated 3 times. The error bar represents the standard deviation. SEM images of *S. aureus* on the (b) bare LPFGs, (c) $[\text{PAH}/\text{PAA}]_{10}$ -PAH-coated LPFGs and (d) nanoporous coated LPFGs at 60 min. The inset of (d) is a zoomed-in SEM image of *S. aureus* attached to the nanoporous $[\text{PAH}/\text{PAA}]_{10}$ -PAH-coated LPFG at 60 min.

Because *S. aureus* were detected using the LPFGs with various functional coatings, we explored the specificity of this technology using other bacteria. *E. coli* were selected due to their distinctive shape (rod-like), biology (G⁻) and size. Interestingly, the results were quite different from those of *S. aureus*. Figure 4a shows the RW shifts of the bare LPFGs, $[\text{PAH}/\text{PAA}]_{10}$ -PAH-coated LPFGs and nanoporous $[\text{PAH}/\text{PAA}]_{10}$ -PAH-coated LPFGs when monitoring *E. coli*. The fitted slopes were 1.82, 0.29 and $3.76 \text{ pm}/\text{min}$, respectively. As expected, there was an increase in the RW shift of the nanoporous coated LPFGs on *E. coli* detection, perhaps due to the increased surface area by the nanoporous structure and thus the reduced shear stress, leading to bacterial retention on the surface of coatings. The transmission spectra of nanoporous $[\text{PAH}/\text{PAA}]_{10}$ -PAH-coated LPFGs for *E. coli* detection for the first 60 min were shown in Figure S3b. Figure 4b–d are the overall SEM images of *E. coli* on bare LPFGs, $[\text{PAH}/\text{PAA}]_{10}$ -PAH-coated LPFGs and nanoporous $[\text{PAH}/\text{PAA}]_{10}$ -PAH-coated LPFGs at 60 min, respectively. The densities of *E. coli* on various platforms are shown in Figure S2. It shows clearly that the density of *E. coli* attached to the nanoporous coatings (Figure 4d) was higher than that on the bare LPFGs (Figure 4b) and the coated LPFGs (Figure 4c). It was still lower when compared to that of *S. aureus* attached to the nanoporous coatings (Figure 3d). What is surprising is that there was almost no RW shift for the coated LPFGs during *E. coli* detection, which is in contrast to the *S. aureus* detection, indicating the limited adhesion of *E. coli* on the coated LPFG surface. Figure 4c further

demonstrates that there were few *E. coli* attached to the coated LPFG after 60 min, which is consistent with the limited RW shift as shown in Figure 4a (green circle).

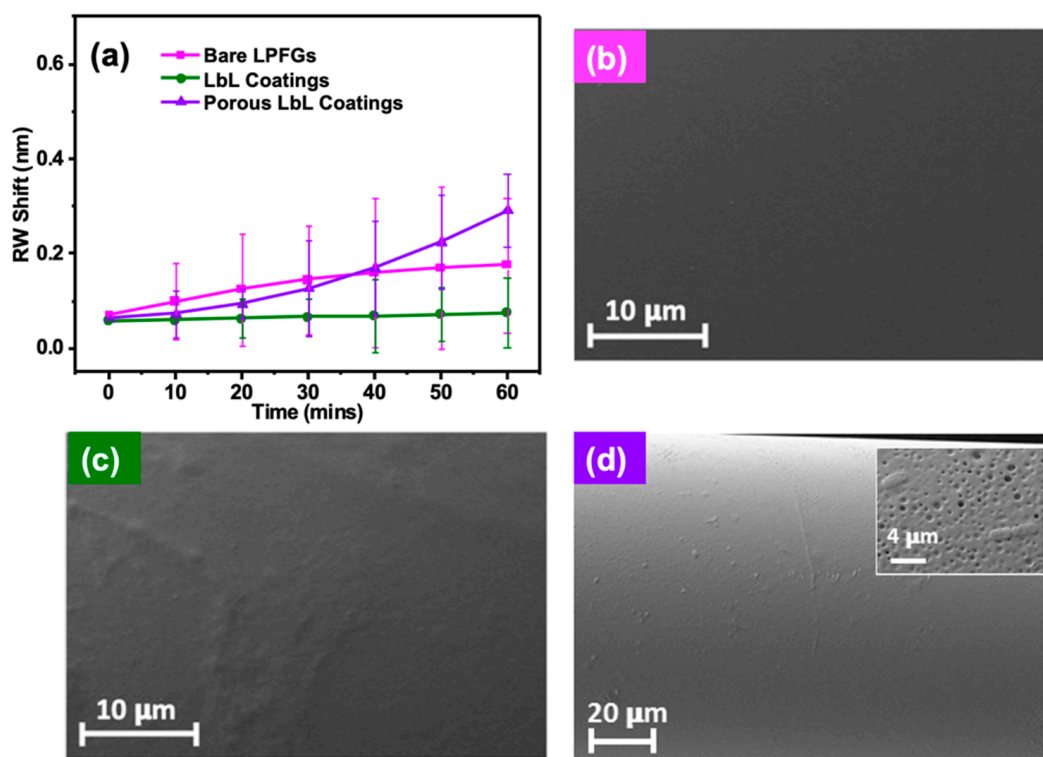


Figure 4. (a) The time-resolved RW shifts of the bare LPFGs, the [PAH/PAA]₁₀-PAH-coated LPFGs and the nanoporous coated LPFGs for *E. coli* detections at a flow rate of 30 $\mu\text{L}/\text{min}$ and temperature of 37 $^{\circ}\text{C}$ for 60 min. Each experiment was repeated 3 times. The error bar represents standard deviation. SEM images of *E. coli* on the (b) bare LPFGs, (c) [PAH/PAA]₁₀-PAH-coated LPFGs and (d) nanoporous [PAH/PAA]₁₀-PAH-coated LPFGs at 60 min. The inset of (d) is a zoomed-in SEM image of *E. coli* attached to the nanoporous coated LPFG at 60 min.

The results of the RW shifts of LPFGs with different coatings for 60 min in *S. aureus* bacterial solution are summarized in Table 1. As recorded in Table 1, the ratio of the RW shifts for *S. aureus* detection between the bare LPFGs, the [PAH/PAA]₁₀-PAH-coated LPFGs and the nanoporous [PAH/PAA]₁₀-PAH-coated LPFGs was 1:4.08:7.09.

Table 1. The ratio of the RW shifts between different LPFG-based platforms in *S. aureus* PBS solutions with concentration of 10^4 CFU/mL at 60 min.

Substrate	<i>S. aureus</i> Detection at 60 min	
	RW Shift (nm)	Ratio of RW Shift between Various Platforms
Bare LPFG	0.07 ± 0.05	1
[PAH-PAA] ₁₀ -PAH LbL-coated LPFG	0.31 ± 0.14	4.08
Porous [PAH-PAA] ₁₀ -PAH LbL-coated LPFG	0.53 ± 0.21	7.09

However, the ratio of the RW shifts for *E. coli* detection for 60 min between the bare LPFGs, the [PAH/PAA]₁₀-PAH-coated LPFGs and the nanoporous [PAH/PAA]₁₀-PAH-coated LPFGs was 1:0.31:1.13, as shown in Table S1. Unlike *S. aureus* with its striking increase in RW shifts (4.08:1), there is an obvious decrease in the RW shifts for *E. coli* detection (0.31:1) using coated LPFGs compared to using bare LPFGs. This is highly likely

due to the inherent hydrophobic property of *E. coli* [48]. The surface of *E. coli* is composed of lipopolysaccharides with a rigid framework and an inevitable steric hindrance. Moreover, the pili of *E. coli* collide with the substrate during detection, and so the mechanical resistance of the substrate material to pili retraction would increase with increasing substrate stiffness; this means the adhesion of *E. coli* on a stiffer substrate (such as bare LPFGs) could increase the lifetime of pili–substrate interactions [49]. This is in contrast to *S. aureus*, which does not possess pili. Furthermore, the outer layer of the LbL coatings comprises PAH with a pH of 7.5, which is less than the pKa of PAH (pKa is 8.5). This indicates that the PAH layers have protonated amino groups. Compared with *S. aureus*, these uncharged amines are more lethal to the more negatively charged *E. coli* [50] and thus, the adhesion of *E. coli* on LbL coatings would decrease. As a result, the RW shift of *E. coli* on LbL coatings is almost zero, which is even smaller than that of the bare LPFGs. There is an appreciable increase in the RW shift when using nanoporous coated LPFGs compared to bare LPFGs for *S. aureus* detections (1:7.09), however, the effect of the nanoporous coatings on the RW shift for *E. coli* detections was not obvious (1:1.13). This drastic difference inspired us to explore the potential of various coating strategies to differentiate the two bacteria.

2.3. Bacterial Differentiation Using Functional Coatings on LPFGs

To demonstrate the potential of the LbL coatings with or without nanostructured pores for the differentiation of *S. aureus* and *E. coli*, the transmission spectra were recorded up to 260 min. Figure 5a shows the RW shifts of the bare LPFGs in *S. aureus* and *E. coli* PBS solutions over this duration. The fitted slopes of the two curves corresponding to *S. aureus* and *E. coli* adhesions were similar, at 0.92 and 1.04 pm/min, respectively. Figure 5b shows that there was a drastic difference in the RW shifts of the [PAH/PAA]₁₀-PAH-coated LPFGs in response to the presence of *S. aureus* and *E. coli*. The fitted slopes of the RW shifts for *S. aureus* and *E. coli* were 5.31 and 0.58 pm/min, respectively. As explained in the previous section, this is possibly because *S. aureus* is more hydrophilic [45] than *E. coli* and so is more able to attach to the LbL coatings. The RW shifts of the nanoporous [PAH/PAA]₁₀-PAH-coated LPFGs for *S. aureus* and *E. coli* adhesion for 260 min are shown in Figure 5c. When the nanoporous structures were introduced in the coatings, the fitted slope for *S. aureus* increased to 9.96 pm/min. However, for *E. coli* detection, although the slope of the RW shift increased in the first 60 min because of the reduction in shear stress caused by the nanoporous structure, and therefore protection and retention of bacteria occurred, it plateaued over a longer period, with a slope as low as 2.63 pm/min. As discussed in Section 2.2, this is conceivably due to the hydrophobicity of the *E. coli* surface and the antibacterial properties selected for the PAH-layer coatings, which lead to a decrease in *E. coli* adhesion on the functional coatings.

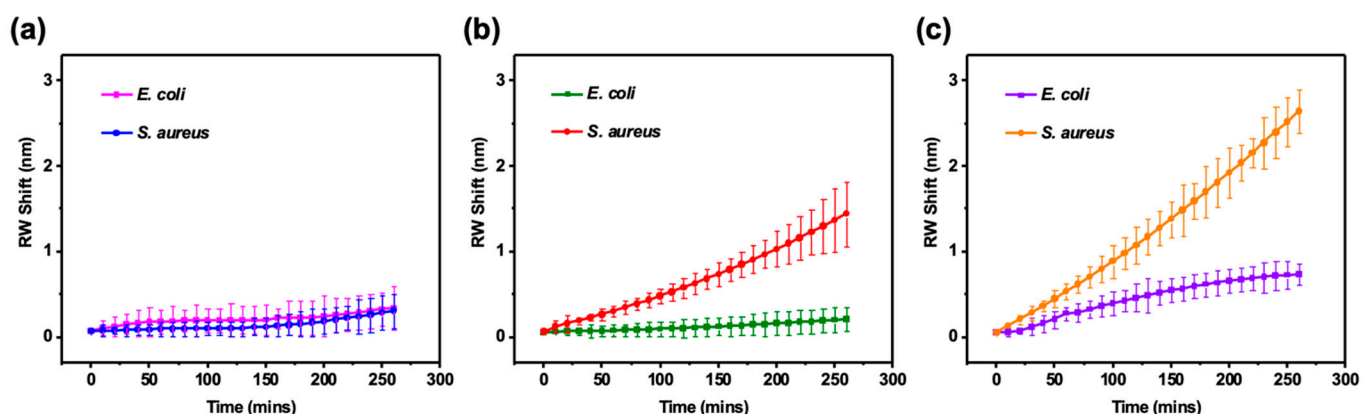


Figure 5. The time-resolved RW shifts of the (a) bare LPFGs, (b) [PAH/PAA]₁₀-PAH-coated LPFGs and (c) porous [PAH/PAA]₁₀-PAH-coated LPFGs in 10⁴ CFU/mL *S. aureus* and *E. coli* PBS solutions at a flow rate of 30 μL/min and temperature of 37 °C for 260 min.

Figure 6 and Table 2 compare the RW shifts during the monitoring of *S. aureus* and *E. coli* adhesion using LPFGs with various coatings. Figure 6a shows the RW shifts at 60 min. It can be noticed that the RW shift of the bare LPFGs for *E. coli* detection is slightly larger than that for *S. aureus* detection, which can be explained by the *attachment point theory* [47]. The dissimilarities in the adhesion patterns between sphere-shaped *S. aureus* and rod-shaped *E. coli* can be attributed to the discrepancy in the number of available access points for bacteria on polyelectrolyte functional coatings. Figure 6b shows the RW shifts at 260 min. The specific RW shifts are listed in Table 2. At 260 min, the RW shifts of the bare LPFGs, the [PAH/PAA]₁₀-PAH-coated LPFGs and the nanoporous [PAH/PAA]₁₀-PAH-coated LPFGs for *S. aureus* detection are 0.31 ± 0.16 , 1.44 ± 0.33 and 2.64 ± 0.17 nm, respectively. For *E. coli* detection at 260 min, the RW shifts of the bare LPFGs, the [PAH/PAA]₁₀-PAH-coated LPFGs and the nanoporous [PAH/PAA]₁₀-PAH-coated LPFGs are 0.37 ± 0.20 , 0.21 ± 0.11 and 0.74 ± 0.12 nm, respectively. Figure 6a,b shows that for *S. aureus* detection, the RW shifts of the coated LPFGs and the nanoporous coated LPFGs at 260 min were significantly increased compared to that at 60 min. However, for *E. coli* detection at 260 min, the enhancement in RW shifts of the coated LPFGs and the nanoporous coated LPFGs were much lower than that for *S. aureus* detection. For *E. coli* detection, there is an obvious difference in the RW shifts between coated LPFGs and other coating strategies; it was even lower than that of the bare LPFGs.

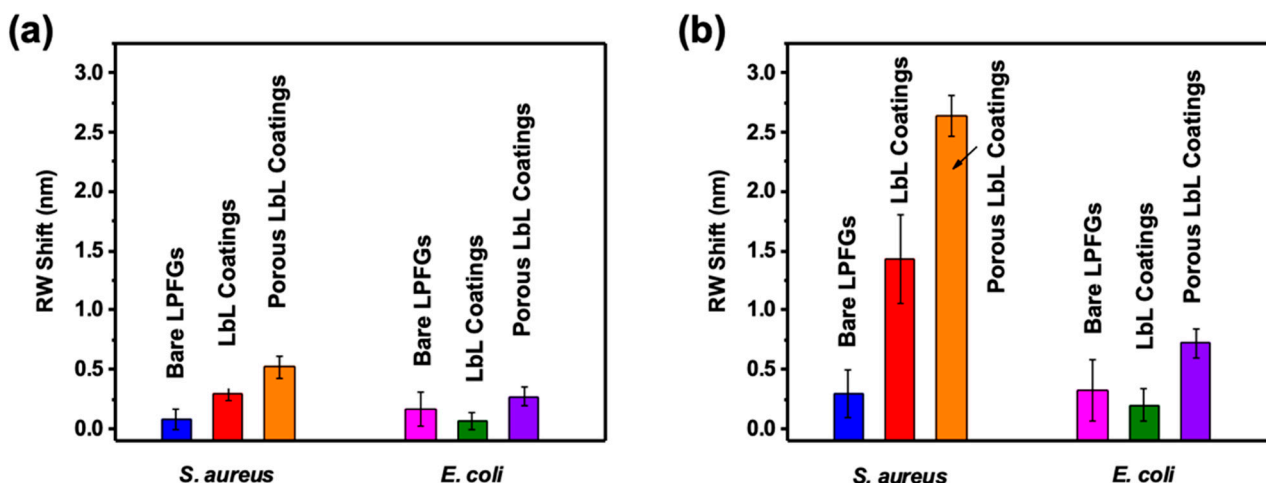


Figure 6. The RW shifts of LPFGs coated with functional coatings on 10^4 CFU/mL *S. aureus* and *E. coli* PBS solutions at a flow rate of $30 \mu\text{L}/\text{min}$ and temperature of 37°C at (a) 60 min and (b) 260 min.

Table 2. The RW shifts of the functional coatings on LPFGs in 10^4 CFU/mL *S. aureus* and *E. coli* solutions at 260 min and the ratios between the RW shifts for *S. aureus* and *E. coli* detections at 260 and 60 min.

Substrate	RW Shift at 260 min (nm)		Ratio of RW Shift: <i>S. aureus</i> : <i>E. coli</i>	
	<i>S. aureus</i>	<i>E. coli</i>	260 min	60 min
Bare LPFG	0.31 ± 0.16	0.37 ± 0.20	0.83:1	0.31:1
[PAH/PAA] ₁₀ -PAH LbL-coated LPFG	1.44 ± 0.33	0.21 ± 0.11	6.89:1	4.00:1
Porous [PAH/PAA] ₁₀ -PAH LbL-coated LPFG	2.64 ± 0.17	0.74 ± 0.12	3.60:1	1.92:1

In order to illustrate the optimal conditions for differentiation between *S. aureus* and *E. coli*, the ratios of the RW shifts for *S. aureus* and *E. coli* detection using the three coating strategies after 60 and 260 min adhesion are provided in the last two columns of Table 2; all variations of the ratio with time were recorded in Table S2. As recorded in Table 2, at 60 min, the ratios between the RW shifts for the detections of *S. aureus* and *E. coli* were 0.31:1, 4.00:1 and 1.92:1 for the bare LPFGs, the [PAH/PAA]₁₀-PAH-coated LPFGs and the nanoporous [PAH/PAA]₁₀-PAH-coated LPFGs, respectively. These ratios increased to 0.83:1, 6.89:1 and 3.60:1 at an extended time of 260 min, respectively. A higher ratio indicates better differentiation between the two types of bacteria.

Among the three coating strategies, the coated LPFGs exhibited overall higher ratio and thus a better differentiation. The best differentiation was achieved for coated LPFGs at 260 min, with the highest ratio of 6.89:1. In order to maximize the ability to differentiate, it is necessary to extend the adhesion and detection time.

3. Conclusions

In this study, a novel approach has been described for expeditious bacterial detection of *S. aureus* utilizing LPFGs that are integrated with functional polyelectrolyte coatings featuring meticulously designed nanoporous structures. The LbL assembly allows the deposition of polyelectrolyte coatings with high-quality thickness on the LPFG surface. The functional polyelectrolyte coatings, characterized by their nanoporous structure, were grown and integrated with the LPFG platform to facilitate the rapid detection of bacteria by increasing its adhesion on the surface of the functional coatings. Since this is effected by the size of the nanoporous structure, future work should design different sizes and shapes of nanopores to further investigate and explore bacterial detection and differentiation. The RW shift of [PAH/PAA]₁₀-PAH-coated and nanoporous coated LPFGs was increased by ~4- and 7-fold, respectively, compared to that of bare LPFGs for *S. aureus* detection at 60 min. The nanoporous coated LPFG is thus suitable for swift detection of *S. aureus*. The capability of LPFGs with various functional coatings for *E. coli* detection was also explored with the coated LPFGs showing the lowest RW shift, which is in contrast to that of the *S. aureus*, perhaps due to the different adhesion behaviors of the two bacteria on the polyelectrolyte coatings. Based on the drastically different LPFG response to *S. aureus* and *E. coli*, we further explored and demonstrated the potential in bacterial differentiation using LPFGs with various functional coatings. The flexibility in fabricating and controlling the nanostructure of functional polyelectrolyte coatings on the LPFG makes our biosensor platform robust for rapid bacterial detection as well as differentiation. This study set up a good foundation for us to further explore multi-culture detection in the future.

4. Experimental Section

4.1. Chemical Reagents and Materials

Sodium hydroxide standard solution (0.1 M, NaOH), sodium chloride (NaCl), potassium chloride (KCl), sodium dihydrogen phosphate (NaH₂PO₄), disodium phosphate (Na₂HPO₄), poly(allylamine hydrochloride) (PAH, Mw ~17.5 kDa), poly(acrylic acid) (PAA, Mw ~450 kDa), tryptic soy broth (TSB), glucose, agar, nitric acid and glutaraldehyde were purchased from Sigma-Aldrich (St. Louis, MO, USA). Hydrochloric acid (1N standard solution, HCl) was obtained from Acros Organics (Geel, Belgium). *Staphylococcus aureus* (ATCC[®] 29213[™], Gram-positive) and *Escherichia coli* (ATCC[®] 25404[™], Gram-negative) were purchased from American Type Culture Collection (ATCC, Manassas, VA, USA). All chemicals were used without further purification steps. All solutions were prepared using Milli-Q ultrapure water (no less than 18.2 MΩ).

4.2. LPFG Fabrication

The LPFGs were fabricated using point-by-point irradiation of a focused CO₂ laser beam. The CO₂ laser with a closed-loop kit has excellent power stability to ensure the reproducibility of LPFG. The LPFG coupled with LP_{0,10} cladding mode was inscribed in

the SMF-28 optical fiber (from Corning Optical Communications Inc., Charlotte, NC, USA) using the CO₂ laser with a 120° Au-coated Si mirror pair via a motorized movement stage with ~0.2 μm incremental range [51]. The entire fabrication of the LPFG was controlled by a desktop computer interface to ensure synchronized operations of laser irradiation and movement of the stage. The SMF-LPFG was fabricated with a period of 247 μm and a total length of 50 mm. A broadband light source was connected to one end of the LPFG and an optical spectrum analyzer (OSA) was connected to the other for the measurement of the transmission spectra of the LPFG in real time during the fabrication process [52].

4.3. Preparation of [PAH/PAA]₁₀-PAH Coatings

As illustrated in Figure S1, the LPFG was positioned in a straight orientation between two stable holders on a motorized arm, then immersed into 0.1 M NaOH standard solution for 20 min in order to clean the surface. Then, it was dipped into containers filled with alternative polymer solutions and subsequently into rinsing phosphate-buffered saline (PBS) solution during the LbL self-assembly cycles at room temperature. During the entire deposition process, the PAH solution was pH-adjusted to pH 7.5, and the PAA solution was pH-adjusted to pH 3.5. The rinsing PBS buffer solution was kept at pH 7.4. Specifically, the LPFG was immersed into the PAH solution with a concentration of 0.2 mg/mL for 10 min, followed by a rinsing step in 0.1 M PBS buffer solution for 5 min, and subsequently immersed into the 0.2 mg/mL PAA solution for 10 min, followed by the same rinsing step. The above deposition process was repeated 10 times to prepare 10 bilayers of [PAH/PAA], and the last step involved depositing a PAH layer to form the [PAH/PAA]₁₀-PAH polyelectrolyte coating on the surface of the LPFG. Upon completion of the coating process, the coated LPFG was dried in an oven at 200 °C for a duration of 30 min. Subsequently, the LPFGs with [PAH/PAA]₁₀-PAH coatings were stored under ambient conditions prior to measurement.

4.4. Preparation of Nanoporous [PAH/PAA]₁₀-PAH Coatings

The LPFG with [PAH/PAA]₁₀-PAH coatings prepared in Section 4.3 was dipped into 0.01 M NaH₂PO₄ solution for 5 s (pH adjusted to 5.0), followed by three consecutive dipping steps in NaH₂PO₄ buffer solution at pH 4.0 for 5 s, NaH₂PO₄ buffer solution at pH 3.3 for 1 min and NaH₂PO₄ buffer solution at pH 2.5 for 5 min. Then, it was rinsed with PBS buffer solution at pH 7.4 for 10 min and blown dry. LPFGs with Nanoporous [PAH/PAA]₁₀-PAH coatings were stored under ambient conditions before measurement.

4.5. Culture and Preparation of *S. aureus* and *E. coli*

A single isolated colony of bacteria (*S. aureus* or *E. coli*) was picked from an agar plate, and then transferred into a 50 mL conical tube containing ~10 mL trypsin soy broth with 0.2% glucose (TSBG) medium. The sample was incubated with orbital agitation (175 rpm) at 37 °C for 18 h. A small amount of incubated bacteria was diluted with fresh TSBG medium and grown for additional 2–3 h to reach the mid-exponential growth phase. The bacteria culture was centrifuged for 10 min at 1500 rpm in a 15 mL centrifuge tube and resuspended with saline to the initial optical cell density of 0.29 ± 0.02 at 570 nm (OD 570) measured by a Unico® (Bohemia, NY, USA) 1100 spectrophotometer (the bacterial concentration was 10^8 to 2×10^8 cells/mL). The broth was then serially diluted 10^4 times with PBS to a final concentration of 10^4 to 2×10^4 cells/mL.

4.6. Characterization and Analysis

The size of the nanoporous structure and the bacteria attached to the surface of the LPFG with various functional coatings were characterized using a Scanning Electron Microscope (SEM) at 3 kV accelerating voltage, with a working distance of 7.5 mm, utilizing an Auriga Modular Cross Beam workstation from Carl Zeiss, Inc. (Thornwood, NY, USA). The SEM images were analyzed using ImageJ 1.52 software from the National Institutes of Health.

4.7. Optofluidic Platform

An all-optical lab-on-fiber optofluidic platform (LOFOP) was designed and developed for in situ measurements in the biological micro-environment [29]. It was composed of two vital and multifunctional components. One part comprised the LPFG as a sensing element, and the other was a glass capillary to allow bacterial adhesion on the LPFG under continuous flow conditions. The LPFG and the glass capillary, with a length of 50 mm and an inner diameter of 1.56 mm, were assembled to create a liquid-tight LOFOP with an inlet and an outlet for flow regulation using a syringe pump (New Era Pump Systems, Inc., Farmingdale, NY, USA). Two ends of the LPFG were fixed as it was mounted in LOFOP. The entire LOFOP setup was placed in an incubator set at a temperature of 37 °C [29]. Each measurement was repeated 3 times.

Supplementary Materials: The following supporting information can be downloaded at: <https://www.mdpi.com/article/10.3390/coatings13040778/s1>. Figure S1: Schematic of the [PAH/PAA]₁₀-PAH coatings self-assembly process; Figure S2: The densities of different bacteria attached on various functional coatings on LPFG in 10⁴ CFU/mL bacteria PBS solution at a flow rate of 30 μL/min and temperature of 37 °C at 60 min. Figure S3: The transmission spectra of porous coatings for (a) *S. aureus* and (b) *E. coli* detection at different time spots. Table S1: The ratio of the RW shifts between different LPFG-based platforms in *E. coli* PBS solutions with concentration of 10⁴ CFU/mL at 60 min. Table S2: The ratios between the RW shifts for *S. aureus* and *E. coli* detections at different time points. References [52–56] are cited in the supplementary materials.

Author Contributions: Conceptualization, S.H. and F.Y.; methodology, S.H., J.W., F.Y. and T.-L.C.; software, S.H., Z.T., K.L. and S.L.; validation, S.H. and K.L.; formal analysis, S.H. and K.L.; investigation, S.H. and J.W.; resources, J.-F.L., H.D. and Y.L.; data curation, S.H., Z.T. and S.L.; writing—original draft, S.H.; writing—review and editing, S.H., F.Y., F.T., J.-F.L., H.D. and Y.L.; visualization, S.H.; supervision, S.H., J.-F.L., H.D. and Y.L.; project administration, H.D.; funding acquisition, F.T., H.D. and Y.L. All authors have read and agreed to the published version of the manuscript.

Funding: This work was supported by the US National Science Foundation [grant number ECCS-1611155] and Hunan Provincial Science and Technology Achievement and Industry Program [grant number 2021GK4014].

Institutional Review Board Statement: Not applicable.

Informed Consent Statement: Not applicable.

Data Availability Statement: Not applicable.

Conflicts of Interest: The authors declare no conflict of interest.

References

1. Smietana, M.; Bock, W.J.; Mikulic, P.; Ng, A.; Chinnappan, R.; Zourob, M. Detection of bacteria using bacteriophages as recognition elements immobilized on long-period fiber gratings. *Opt. Express* **2011**, *19*, 7971. [CrossRef]
2. Zourob, M.; Mohr, S.; Brown, B.J.T.; Fielden, P.R.; McDonnell, M.B.; Goddard, N.J. Bacteria detection using disposable optical leaky waveguide sensors. *Biosens. Bioelectron.* **2005**, *21*, 293–302. [CrossRef] [PubMed]
3. Shabani, A.; Zourob, M.; Allain, B.; Marquette, C.A.; Lawrence, M.F.; Mandeville, R. Bacteriophage-modified microarrays for the direct impedimetric detection of bacteria. *Anal. Chem.* **2008**, *80*, 9475–9482. [CrossRef] [PubMed]
4. Taylor, A.D.; Yu, Q.; Chen, S.; Homola, J.; Jiang, S. Comparison of *E. coli* O157:H7 preparation methods used for detection with surface plasmon resonance sensor. *Sens. Actuators B Chem.* **2005**, *107*, 202–208. [CrossRef]
5. Templier, V.; Roux, A.; Roupioz, Y.; Livache, T. Ligands for label-free detection of whole bacteria on biosensors: A review. *TrAC-Trends Anal. Chem.* **2016**, *79*, 71–79. [CrossRef]
6. Wang, T.; Liu, J.; Gu, X.; Li, D.; Wang, J.; Wang, E. Label-free electrochemical aptasensor constructed by layer-by-layer technology for sensitive and selective detection of cancer cells. *Anal. Chim. Acta* **2015**, *882*, 32–37. [CrossRef]
7. Cho, I.; Blaser, M.J. The human microbiome: At the interface of health and disease. *Nat. Rev. Genet.* **2012**, *13*, 260–270. [CrossRef]
8. Bock, W.J.; Tripathi, S.M.; Smietana, M. Sensitive and Selective Lab-on-a-Fiber Sensor for Bacteria Detection in Water. *Springer Ser. Surf. Sci.* **2015**, *56*, 315–334.
9. Baeumner, A.J.; Cohen, R.N.; Miksic, V.; Min, J. RNA biosensor for the rapid detection of viable *Escherichia coli* in drinking water. *Biosens. Bioelectron.* **2003**, *18*, 405–413. [CrossRef]

10. Van Dorst, B.; Mehta, J.; Bekaert, K.; Rouah-Martin, E.; De Coen, W.; Dubruel, P.; Blust, R.; Robbens, J. Recent advances in recognition elements of food and environmental biosensors: A review. *Biosens. Bioelectron.* **2010**, *26*, 1178–1194. [[CrossRef](#)]
11. Balasubramanian, S.; Sorokulova, I.B.; Vodyanoy, V.J.; Simonian, A.L. Lytic phage as a specific and selective probe for detection of *Staphylococcus aureus*—A surface plasmon resonance spectroscopic study. *Biosens. Bioelectron.* **2007**, *22*, 948–955. [[CrossRef](#)] [[PubMed](#)]
12. Arora, P.; Sindhu, A.; Dilbaghi, N.; Chaudhury, A. Biosensors as innovative tools for the detection of food borne pathogens. *Biosens. Bioelectron.* **2011**, *28*, 1–12. [[CrossRef](#)]
13. Rijal, K.; Leung, A.; Shankar, P.M.; Mutharasan, R. Detection of pathogen *Escherichia coli* O157:H7 at 70 cells/mL using antibody-immobilized biconical tapered fiber sensors. *Biosens. Bioelectron.* **2005**, *21*, 871–880. [[CrossRef](#)] [[PubMed](#)]
14. Lu, X.; Samuelson, D.R.; Xu, Y.; Zhang, H.; Wang, S.; Rasco, B.A.; Xu, J.; Konkel, M.E. Detecting and tracking nosocomial methicillin-resistant *Staphylococcus aureus* using a microfluidic SERS biosensor. *Anal. Chem.* **2013**, *85*, 2320–2327. [[CrossRef](#)]
15. Yang, F.; Chang, T.-L.; Liu, T.; Wu, D.; Du, H.; Liang, J.; Tian, F. Label-free detection of *Staphylococcus aureus* bacteria using long-period fiber gratings with functional polyelectrolyte coatings. *Biosens. Bioelectron.* **2019**, *133*, 147–153. [[CrossRef](#)]
16. Goodridge, L.; Chen, J.; Griffiths, M. Development and characterization of a fluorescent-bacteriophage assay for detection of *Escherichia coli* O157:H7. *Appl. Environ. Microbiol.* **1999**, *65*, 1397–1404. [[CrossRef](#)]
17. Liu, K.; Chen, T.; He, S.; Robbins, J.P.; Podkolzin, S.G.; Tian, F. Observation and Identification of an Atomic Oxygen Structure on Catalytic Gold Nanoparticles. *Angew. Chem.-Int. Ed.* **2017**, *56*, 12952–12957. [[CrossRef](#)] [[PubMed](#)]
18. Liu, K.; He, S.; Li, L.; Liu, Y.; Huang, Z.; Liu, T.; Wu, H.; Jiang, X.; Liu, K.; Tian, F. Spectroscopically clean Au nanoparticles for catalytic decomposition of hydrogen peroxide. *Sci. Rep.* **2021**, *11*, 9709. [[CrossRef](#)]
19. He, S.; Wu, D.; Chen, S.; Liu, K.; Yang, E.-H.; Tian, F.; Du, H. Au-on-Ag nanostructure for in-situ SERS monitoring of catalytic reactions. *Nanotechnology* **2022**, *33*, 155701. [[CrossRef](#)] [[PubMed](#)]
20. Tang, Z.; Chen, T.; Liu, K.; Du, H.; Podkolzin, S.G. Atomic, Molecular and Hybrid Oxygen Structures on Silver. *Langmuir* **2021**, *37*, 11603–11610. [[CrossRef](#)] [[PubMed](#)]
21. Scoullou, E.V.; Hofman, M.S.; Zheng, Y.; Potapenko, D.V.; Tang, Z.; Podkolzin, S.G.; Koel, B.E. Guaiacol Adsorption and Decomposition on Platinum. *J. Phys. Chem. C* **2018**, *122*, 29180–29189. [[CrossRef](#)]
22. Zheng, Y.; Tang, Z.; Podkolzin, S.G. Catalytic Platinum Nanoparticles Decorated with Subnanometer Molybdenum Clusters for Biomass Processing. *Chem.-A Eur. J.* **2020**, *26*, 5174–5179. [[CrossRef](#)]
23. Robbins, J.P.; Ezeonu, L.; Tang, Z.; Yang, X.; Koel, B.E.; Podkolzin, S.G. Propane Dehydrogenation to Propylene and Propylene Adsorption on Ni and Ni-Sn Catalysts. *ChemCatChem* **2022**, *14*, e202101546. [[CrossRef](#)]
24. Zheng, Y.; Qi, Y.; Tang, Z.; Hanke, F.; Podkolzin, S.G. Kinetics and Reaction Mechanisms of Acetic Acid Hydrodeoxygenation over Pt and Pt-Mo Catalysts. *ACS Sustain. Chem. Eng.* **2022**, *10*, 5212–5224. [[CrossRef](#)]
25. Zheng, Y.; Qi, Y.; Tang, Z.; Tan, J.; Koel, B.E.; Podkolzin, S.G. Spectroscopic observation and structure-insensitivity of hydroxyls on gold. *Chem. Commun.* **2022**, *58*, 4036–4039. [[CrossRef](#)]
26. Ezeonu, L.; Tang, Z.; Qi, Y.; Huo, F.; Zheng, Y.; Koel, B.E.; Podkolzin, S.G. Adsorption, surface reactions and hydrodeoxygenation of acetic acid on platinum and nickel catalysts. *J. Catal.* **2023**, *418*, 190–202. [[CrossRef](#)]
27. Wolfbeis, O.S. Fiber-optic chemical sensors and biosensors. *Anal. Chem.* **2006**, *78*, 3859–3873. [[CrossRef](#)]
28. Helmerhorst, E.; Chandler, D.J.; Nussio, M.; Mamotte, C.D. Real-time and label-free bio-sensing of molecular interactions by surface plasmon resonance: A laboratory medicine perspective. *Clin. Biochem. Rev.* **2012**, *33*, 161–173.
29. Bandara, A.B.; Zuo, Z.; Ramachandran, S.; Ritter, A.; Heflin, J.R.; Inzana, T.J. Detection of methicillin-resistant staphylococci by biosensor assay consisting of nanoscale films on optical fiber long-period gratings. *Biosens. Bioelectron.* **2015**, *70*, 433–440. [[CrossRef](#)]
30. Boudou, T.; Crouzier, T.; Ren, K.; Blin, G.; Picart, C. Multiple functionalities of polyelectrolyte multilayer films: New biomedical applications. *Adv. Mater.* **2010**, *22*, 441–467. [[CrossRef](#)]
31. Saha, N.; Monge, C.; Dulong, V.; Picart, C.; Glinel, K. Influence of polyelectrolyte film stiffness on bacterial growth. *Biomacromolecules* **2013**, *14*, 520–528. [[CrossRef](#)] [[PubMed](#)]
32. Yang, F.; Kanka, J.; Tian, F. Silica nanoparticle coated long-period grating for in situ monitoring of drug delivery thin films. *Opt. Fibers Sens. Med. Diagn. Treat. Appl. XVII* **2017**, *10058*, 1005809.
33. Hammond, P.T. Building biomedical materials layer-by-layer. *Mater. Today* **2012**, *15*, 196–206. [[CrossRef](#)]
34. Du, Y.; Chen, C.; Li, B.; Zhou, M.; Wang, E.; Dong, S. Layer-by-layer electrochemical biosensor with aptamer-appended active polyelectrolyte multilayer for sensitive protein determination. *Biosens. Bioelectron.* **2010**, *25*, 1902–1907. [[CrossRef](#)]
35. Tang, Z.; Wang, Y.; Podsiadlo, P.; Kotov, N.A. Biomedical applications of layer-by-layer assembly: From biomimetics to tissue engineering. *Adv. Mater.* **2006**, *18*, 3203–3224. [[CrossRef](#)]
36. Chiavaioli, F.; Biswas, P.; Trono, C.; Bandyopadhyay, S.; Giannetti, A.; Tombelli, S.; Basumallick, N.; Dasgupta, K.; Baldini, F. Towards sensitive label-free immunosensing by means of turn-around point long period fiber gratings. *Biosens. Bioelectron.* **2014**, *60*, 305–310. [[CrossRef](#)]
37. Mendelsohn, J.D.; Barrett, C.J.; Chan, V.V.; Pal, A.J.; Mayes, A.M.; Rubner, M.F. Fabrication of microporous thin films from polyelectrolyte multilayers. *Langmuir* **2000**, *16*, 5017–5023. [[CrossRef](#)]

38. Sun, B.; Flessner, R.M.; Saurer, E.M.; Jewell, C.M.; Fredin, N.J.; Lynn, D.M. Characterization of pH-induced changes in the morphology of polyelectrolyte multilayers assembled from poly(allylamine) and low molecular weight poly(acrylic acid). *J. Colloid Interface Sci.* **2011**, *355*, 431–441. [[CrossRef](#)]
39. Perera-Costa, D.; Bruque, J.M.; González-Martín, M.L.; Gómez-García, A.C.; Vadillo-Rodríguez, V. Studying the influence of surface topography on bacterial adhesion using spatially organized microtopographic surface patterns. *Langmuir* **2014**, *30*, 4633–4641. [[CrossRef](#)]
40. Whitehead, K.A.; Colligon, J.; Verran, J. Retention of microbial cells in substratum surface features of micrometer and sub-micrometer dimensions. *Colloids Surf. B Biointerfaces* **2005**, *41*, 129–138. [[CrossRef](#)]
41. Harris, J.J.; DeRose, P.M.; Bruening, M.L. Synthesis of passivating, nylon-like coatings through cross-linking of ultrathin polyelectrolyte films. *J. Am. Chem. Soc.* **1999**, *121*, 1978–1979. [[CrossRef](#)]
42. Chang, T.L.; Zhou, X.; Liang, J. Synthesis and characterization of Ag-Cu alloy nanoparticles for antimicrobial applications: A polydopamine chemistry application. *Mater. Sci. Eng. C* **2019**, *98*, 675–684. [[CrossRef](#)]
43. Vaamonde, G.; Chirife, J. Effect of phosphate buffer on *Staphylococcus aureus* growth at a reduced water activity. *Int. J. Food Microbiol.* **1986**, *3*, 51–55. [[CrossRef](#)]
44. Guo, S.; Zhu, X.; Loh, X.J. Controlling cell adhesion using layer-by-layer approaches for biomedical applications. *Mater. Sci. Eng. C* **2017**, *70*, 1163–1175. [[CrossRef](#)] [[PubMed](#)]
45. Lerebour, G.; Cupferman, S.; Bellon-Fontaine, M.N. Adhesion of *Staphylococcus aureus* and *Staphylococcus epidermidis* to the Episkin®reconstructed epidermis model and to an inert 304 stainless steel substrate. *J. Appl. Microbiol.* **2004**, *97*, 7–16. [[CrossRef](#)] [[PubMed](#)]
46. Trunk, T.; Khalil, H.S.; Leo, J.C. Bacterial autoaggregation. *AIMS Microbiol.* **2018**, *4*, 140–164. [[CrossRef](#)] [[PubMed](#)]
47. Berne, C.; Ellison, C.K.; Ducret, A.; Brun, Y.V. Bacterial adhesion at the single-cell level. *Nat. Rev. Microbiol.* **2018**, *16*, 616–627. [[CrossRef](#)]
48. Jacobson, S.H.; Tullus, K.; Brauner, A. Hydrophobic properties of *Escherichia coli* causing acute pyelonephritis. *J. Infect.* **1989**, *19*, 17–23. [[CrossRef](#)]
49. Lichter, J.A.; Thompson, M.T.; Delgadillo, M.; Nishikawa, T.; Rubner, M.F.; Van Vliet, K.J. Substrata Mechanical Stiffness Can Regulate Adhesion of Viable Bacteria. *Biomacromolecules* **2008**, *9*, 1571–1578. [[CrossRef](#)]
50. Lichter, J.A.; Rubner, M.F. Polyelectrolyte multilayers with intrinsic antimicrobial functionality: The importance of mobile polycations. *Langmuir* **2009**, *25*, 7686–7694. [[CrossRef](#)] [[PubMed](#)]
51. Ivanov, O.V.; Yang, F.; Tian, F.; Du, H. Thin-core fiber structures with overlays for sensing applications. *Opt. Express* **2017**, *25*, 31197. [[CrossRef](#)]
52. Yang, F.; Sukhishvili, S.; Du, H.; Tian, F. Marine salinity sensing using long-period fiber gratings enabled by stimuli-responsive polyelectrolyte multilayers. *Sens. Actuators B Chem.* **2017**, *253*, 745–751. [[CrossRef](#)]
53. Tian, F.; Kanka, J.; Zou, B.; Chiang, K.S.; Du, H. Long-period gratings inscribed in photonic crystal fiber by symmetric CO₂ laser irradiation. *Opt. Express* **2013**, *21*, 13208. [[CrossRef](#)]
54. Vengsarkar, A.M.; Lemaire, P.J.; Judkins, J.B.; Bhatia, V.; Erdogan, T.; Sipe, J.E. Long-period fiber gratings as band-rejection filters. *J. Light. Technol.* **1996**, *14*, 58–64. [[CrossRef](#)]
55. Yang, F.; Hlushko, R.; Wu, D.; Sukhishvili, S.A.; Du, H.; Tian, F. Ocean Salinity Sensing Using Long-Period Fiber Gratings Functionalized with Layer-by-Layer Hydrogels. *ACS Omega* **2019**, *4*, 2134–2141. [[CrossRef](#)]
56. Tian, F.; Kaňka, J.; Yang, F.; Min, J.; Hammond, P.T. Role of silica nanoparticles in monitoring and prolonging release of drug-eluting polyelectrolyte coatings using long-period fiber grating platform. *Sens. Actuators B Chem.* **2017**, *252*, 831–839. [[CrossRef](#)]

Disclaimer/Publisher’s Note: The statements, opinions and data contained in all publications are solely those of the individual author(s) and contributor(s) and not of MDPI and/or the editor(s). MDPI and/or the editor(s) disclaim responsibility for any injury to people or property resulting from any ideas, methods, instructions or products referred to in the content.